HEFAT2011
8th International Conference on Heat Transfer, Fluid Mechanics and Thermodynamics
26 June – 1 July 2011
Pointe Aux Piments, Mauritius

COMPARISON OF FROSTING, DEFROSTING AND CONDENSATE RETENTION CHARACTERISTICS OF VERTICAL PARALLEL MICROGROOVED AND PLAIN BRASS SURFACES IN FORCED CONVECTION CONDITION

Rahman M. A.* and Jacobi A. M.
*Author for correspondence
Department of Mechanical Science and Engineering
University of Illinois at Urbana-Champaign,
Urbana 61801
Illinois, USA,
E-mail: rahman5@illinois.edu

ABSTRACT

In the present study, condensation, frosting and condensate (frost melt water) retention characteristics of brass surfaces with parallel microgrooves have been investigated experimentally and compared with the plain baseline surface. Parallel micro-scale surface features were obtained by a mechanical micromachining process (micro end-milling) without applying any chemical means to modify the surface energy. The surfaces exhibited anisotropic wettability with high static contact angles (SCA) of 132^0 to about 146^0 in the direction parallel to grooves. Frost was grown on sample surfaces (45 mm x 45 mm) inside a thermally controlled chamber, in the presence of very cold surrounding air (≈ -6^0C) under forced convection condition (air velocity of 0.25~1.0 m/s). Condensation and frosting pattern as well as condensate retention characteristics of the microgrooved surfaces were found to be significantly different than on the flat brass surfaces. Highly improved condensate drainage behavior was obtained for the microgrooved surfaces which drained up to 70% more condensate than the flat baseline. It was found that variation in the wettability (static contact angle) of the microgrooved surfaces significantly affects the condensate drainage characteristics. Improved condensate drainage was achieved for surfaces with higher static contact angle and lower wetting anisotropy. Variation of operating parameters (plate temperature, frost surface temperature etc.) during defrosting at different heating rate was also investigated. The findings of the present work provide valuable information on the frosting/defrosting characteristics of microgrooved surfaces signifying its possibility for better condensate management in a broad range of air conditioning, refrigeration and cryogenic applications.

INTRODUCTION

Frost formation on any solid surface, for example, the surface of a heat exchanger occurs when following two conditions are met – solid surface temperature is lower than dew point of the surrounding air and when it is also below the freezing point of water. It is very common phenomenon in most refrigeration, air conditioning and cryogenic applications. Frosting is undesirable for many reasons (all of which involves degradation of the heat exchanger performance and increase in operating cost) and therefore defrosting process is carried out which basically involves supplying heat to the heat transfer to melt the frost and to remove it from the surface. Defrosting has to be done in a periodic manner as some condensate retains on the surface after defrosting and frost forms again on the surface in the next heat transfer cycle. Very frequent defrosting is not desirable because not only the efficiency of the heat exchanger deteriorates, but also the overall operating cost increases due to the energy expenditure associated with the defrosting process.

Surfaces with anisotropic wetting and techniques to modify the wetting behaviour have gained considerable attention in the recent years. Anisotropic wetting refers to the preferential spreading of a liquid drop in certain direction on a surface and is very important in a wide range of applications [1-3]. Wetting behaviour of a surface is usually modified by changing the surface topography or changing the surface free energy by chemical treatment and/or a combination of both [4-9].

The factors affecting the frost formation process on a cold surface are many and are studied widely. Effect of changing the surface energy or wettability of the surface by micro-scale roughness on the frosting/defrosting phenomenon has also been studied by researchers [10-14]. Study of frost formation on a vertical or horizontal flat surface under different convection conditions has been studied for a long time because of its obvious importance in numerous applications. No study on the effects of microscale surface roughness produced by topographic modification only on the condensation, frosting and defrosting behaviour could be located. These works [8-9] described the use of various techniques to create parallel grooves on aluminium surface by topographical modification

only (without any chemical treatment) and very encouraging results on condensate drainage enhancement from these surfaces were reported. But they examined the drainage of condensed water droplets only; no test on the frosting/defrosting was reported by the authors of these papers.

Condensed or freezing droplets on a hydrophobic or hydrophilic substrate can have very different wetting behaviour from the behaviour observed for placed or injected droplet on the surface. After conducting a series of studies on substrates with various kinds of chemically patterned microscale surface roughness, Narhe and Beysens [15-16] reported the observed difference and unique characteristics in the wetting pattern on these micro-patterned surfaces. They also identified different stages in the condensation process on the grooved surface and reported the growth pattern of the condensed droplets. The large condensed water droplets in the later part of the condensation process were found to be no longer in Cassie-Baxter wetting [17], but in Wenzel wetting regime [18].

The effect of surface wetting characteristics on the early and mature stage of frost formation was studied by Hoke *et al.* [10]. They found that denser frost layer forms on a lower energy surface than on a higher energy surface. Their findings were in good agreement with some earlier works. Shin *et al.* [11] found that frost formed on the surface with lower dynamic contact angle had higher thermal conductivity and density during the initial stage, but they observed minor differences after a longer frosting period. More recently, Liu *et al.* [13] examined the frost deposition on a super-hydrophobic surface and reported growth of the frost crystals along the parallel direction of the surface on the superhydrophobic surface instead of the normal vertical frost growth as observed on the plain copper surface.

A number of works have been reported on delaying frost formation and minimizing its growth by the application surface coating of different nature [19-21]. But most of the reported studies show poor performance of the hydrophobic or superhydrophobic coatings for repeated frosting cycles and under humid and wet operating condition, especially when the coating is not fully dry after a defrosting period.

Studies on the effects of surface wettability on the drainage of melt water produced by defrosting or melting ice are very rare. Wu and Webb [22] reported unsuccessful attempts to release frost by mechanical vibration from an aluminium surface with hydrophobic and hydrophilic coating. In a relevant work, Jhee *et al.* [14] reported an enhancement of 3.7% and 11.1% in the water drainage and 3.5% and 10.8% in defrosting efficiency for hydrophilic and hydrophobic aluminium heat exchangers respectively.

In the present study we investigated the frosting, defrosting and condensate retention behaviour of a brass surfaces with parallel microgrooves fabricated by micro end-milling process. Frost was formed on these surfaces in the presence of very cold air under forced convection conditions for a specific period and then defrosted by two different defrosting methods. Condensation, frost formation and defrosting patterns on these surfaces have been studied and compared with the baselines by recording images a high speed camera. The effects of anisotropic wettability on the water retention characteristics are investigated. Variation of different operating parameters during the defrosting period is also examined and the preliminary results are reported herein.

EXPERIMENTS

Sample Fabrication

Tests were conducted on a total of 8 (7 microgrooved and 1 flat baseline) brass surfaces in this study. The microgrooved surfaces were fabricated by a mechanical micro end-milling process (by Microlution 310-S, a high performance 3-axis micro-milling machine). The flat baseline surface tested along with the microgrooved samples had an average surface roughness (Ra) of ≈ 100 nm. The grooved samples were fabricated using end tools of 125 μm diameter. The samples were square plates with 45 mm x 45 mm in size and a thickness of 3.175 mm. The samples had equal number (4) of small holes of 2 mm diameter drilled into both side surfaces for inserting the thermocouple probes.

Brass alloy 360 or free cutting brass (alloy mixture of 61.5% Cu, 35.5% Zn, 3% Pb and 0.35% Fe) was selected as the sample material. This alloy of brass was chosen for its very good material properties, especially for its high machinability so that the size and amount of burr formation can be reduced. Before cutting the grooves, the sample surface was made absolutely plain and parallel by using an end mill of larger diameter (≈ 2.3 mm) for the plaining operation. The spindle speed and feed rate for the groove cutting operation used was 50000 rpm and 400 mm/min respectively and depth of cut per tool pass was 12.5 μm. SEM images of the grooved samples are shown in Figure 1. The machining marks on the pillar and groove surfaces and also burrs on the pillar side and top surfaces can be seen clearly from these images.

The microgrooved samples that were fabricated could be classified into 2 different series- fixed groove height and fixed groove spacing. There were 4 samples with a fixed groove height of 60 μm, but the pillar width (groove spacing) was varied from 26 μm to about 190 μm. The fixed groove spacing series had a fixed pillar width or groove spacing of 112 μm and the groove height was varied from 22 μm to 109 μm. All the microgrooved samples had a groove width of 127 μm. Dimensions of the groove geometry parameters were measured using an Alpha-Step IQ profilometer. These measurements were later verified by taking images of the grooves and pillars

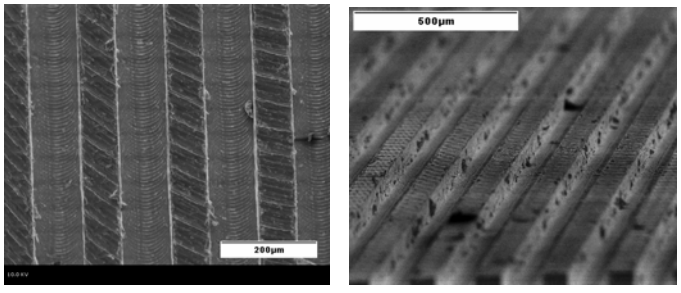

Figure 1 SEM images of micro-grooved brass sample. Machining marks and burrs can be seen on the pillar and groove surfaces

by a very high resolution camera at 20X optical zoom and then dimensions were measured using an image processing software. The maximum uncertainty in the reported groove measurement is within ±5 μm.

Contact angle measurement

The wettability of the prepared samples were characterized by measuring the static contact angle (SCA) on them by sessile drop method using a CAM200 (KSV Instruments) optical goniometer. SCA was measured both in parallel and perpendicular direction of the groove. Measurements were taken at more than 6 different positions on each sample for a range of water droplet volumes inside a class-100 cleanroom facility. The microgrooved samples exhibited very high SCA in parallel direction to the groove compared to the plain brass surface which was hydrophilic in nature (SCA≈ 68^0). SCA on the microgrooved surface ranged from 132.16 to about 145.66^0 in the parallel direction to the groove, while it varied from 27.33^0 to 115.51^0 when viewed from perpendicular direction to the groove. SCA in perpendicular direction was always found to be lower than that in the parallel direction and the anisotropy was as high as 105.33^0.

Experimental Setup

In the present study, all the frosting/defrosting experiments were conducted inside a controlled chamber by cooling the samples using a thermoelectric cooler. The tests were carried out inside the chamber under specific operating conditions, in the presence of very cold air (-5 to -6^0C) and at a relative humidity of ≈ 90±3%. 2D and simplified 3D schematic views of the experimental setup are shown in Figure 2.

The test chamber was a rectangular box of plexi-glass and had a dimension of 12 x 12 x 8.5 in^3. There was a circular view-port at the front-side of the chamber to facilitate the test-time observation and recording of the frosting/defrosting process via a high speed camera (Phantom V60). A cool mist humidifier (Crane, EE-5301) was used to maintain the relative humidity (RH) inside the chamber at the desired value. Relative humidity level of air inside the chamber was measured by 2 hygrometers (measurement uncertainty ±2. A total of eight thermocouples (E-type, uncertainty ± 0.13^0C) were connected to the sample using a high conductivity thermal paste and 4-6 more thermocouples were used to measure air temperature.

Cold air was supplied inside the chamber by a vortex tube cooler (Brand: EXAIR, Model-3225). Cold air flow rate and temperature was controlled by adjusting a slotted valve. Compressed air at 100 psig was supplied to the vortex cooler and the resulting cold air from cooler was fed to the control chamber. Air velocity inside the chamber was 0.3~1.0 m/s (around the sample) which was measured at various points inside the chamber by an anemometer [VelociCalc® 8357, accuracy ±0.01 m/s]. The temperature of the frost surface during frosting and defrosting periods was also measured by an infrared camera [Brand: Mikron Midas, accuracy ±2^0C] at regular intervals.

The mass of accumulated frost and the amount of condensate drained/retained were measured by a direct mass measurement system. The peltier cooler was mounted firmly on a horizontal plexi-glass plate in the back of the chamber and was hung from another horizontal plexi-glass plate on top by two stainless steel columns. The top plexi-glass plate was placed firmly on the top of a precision balance (Mettler XP-6202, accuracy ±0.01 gm). This whole assembly (shafts, horizontal plates and cooler) was placed in such a way that it hangs freely from the balance, without touching any other part of the setup. After mounting the sample on the cooler, the reading on the precision balance was made zero, which ensured that the balance would record the mass of the frost and retained condensate only, during and at the end of the frosting and defrosting tests respectively. As a means of verification, the amount of condensate drained from the sample during the defrosting process was also measured by collecting it on a filter paper and weighing it on another balance with very high precision (Mettler AE 1200, accuracy ±0.001 gm).

Tests were conducted for a plate temperature of – 25^0C. The frosting test was continued for 3 hours which was followed by a defrosting process. During defrosting, cold air supply was switched off and the cover of the control chamber was removed, so defrosting took place in air at room temperature (20±2^0C). The thermo-electric cooler was either switched off or set to the desired defrosting energy input by reversing the connection polarity. Defrost was carried out in two methods. In self-defrost method no external energy was supplied for

Table: 1**:** Dimension of groove geometry and experimental static contact angle values on microgrooved and baseline samples.

Sample	Groove width GW (μm)	Groove height GH (μm)	Aspect ratio (GH/GW)	Pillar width PW (μm)	Static contact angle, θ (^{o})	
					Parallel	Perpendicular
BR-1	127	22	0.17	112	134.71	56.62
BR-2		60	0.47		145.66	85.20
BR-3		88	0.69		142.83	54.15
BR-4		109	0.86		132.67	27.33
BR-5	127	60	0.47	26	139.09	53.05
BR-6				68	132.16	56.57
BR-2				112	145.66	85.20
BR-7				190	142.94	115.51
BL	Plain Baseline (Ra ≈ 100 nm)				68.27	

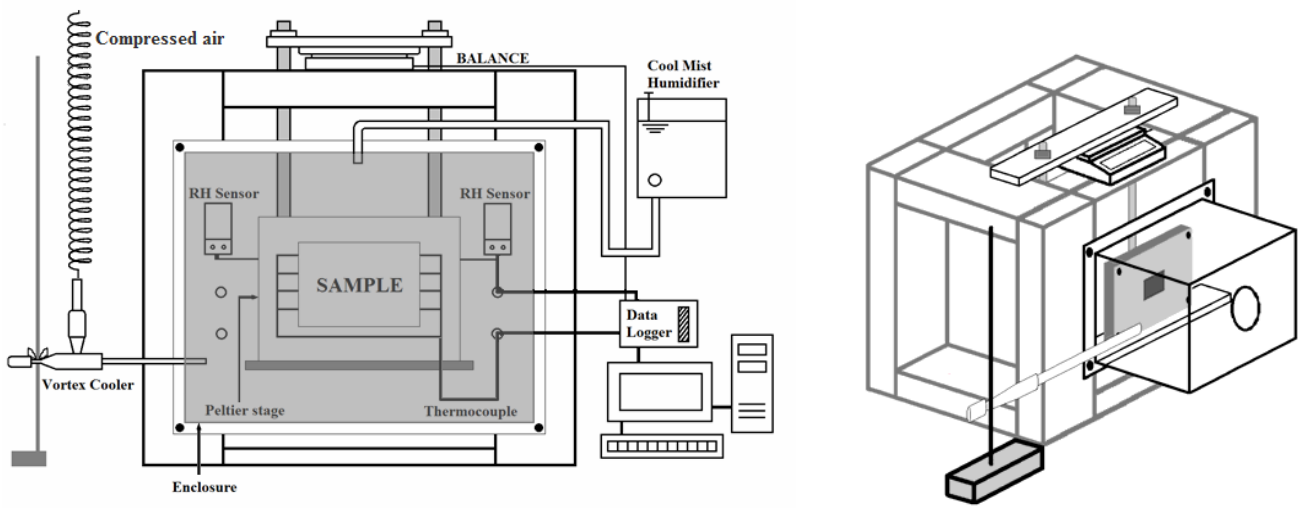

Figure 2 Schematic layout of the experimental setup in (a) 2D and (b) 3D (simplified)

melting the frost and the peltier was simply switched off. In electric defrost method; electric energy was supplied to the substrate at specific power settings. Defrosting process was terminated when all the frost had melted and the plate temperature reached a value of $\approx 5^0$C.

The amount of water drained from the sample during the defrosting process was also measured by collecting it on a filter paper and weighing it over another high precision balance (Mettler AE 1200, accuracy ±0.001 gm). The weight of the sample at the end of the defrosting process was also measured by this second balance as a verification of the measurement values obtained from direct mass measurement.

RESULTS AND DISCUSSION

Frost formation on microgrooved and plain brass surfaces

Frost was grown on the microgrooved and plain brass samples under specific operating conditions (air velocity around the sample ≈ 0.3 ~1.0 m/s, air temperature ≈ -5 to -6^{0}C, plate temperature ≈ -25^{0}C) for 3 hours, which was followed by the defrosting process. To take a closer look at the nature of condensation of water droplets, frost structure and frost formation pattern on the microgrooved and plain brass surfaces, frost was grown on a sample which had microgrooves on its right half and plain baseline on the other half. SCA value of water on the flat surface was ≈ 68^0 and that on the microgrooved portion was ≈ 143^0 and 113^0 when viewed from parallel and perpendicular direction to the grooves respectively. The frost formation process on this sample was recorded by a high speed camera which was equipped with a microscopic zoom-lens. Figure 3 shows a series of images of condensation and frosting process at different time intervals during the frosting process on this sample.

It can be seen from the images of Figure 3 that during the early stage of frost formation and growth, frost structure on both the microgrooved and flat surfaces was very similar under the operating conditions. Droplets of condensed water vapour and consequently frost on the grooved surface formed mostly along the pillar surfaces and the parallel grooves could be seen as black empty lines [Figures 3(a) and 3(b)]. Frost on the other hand, had nearly equal thickness everywhere on the flat surface portion. As the frost deposition on the surface was continued, the grooves became less visible as frost crystals grew in all directions parallel to the surface. From Figure 3(c) it can be seen that frost deposition on the grooved surfaces has occurred and the growth of the frost crystals on the pillars in different directions have covered the empty spaces of the groove surfaces adjacent to them. The frost formed on the microgrooved portion was observed to have a different structure and pattern due to the difference in frost thickness on the pillar and groove surface and as a result, had a less dense structure overall, with empty looking spaces between the pillars. After a frosting period of an hour, frost pattern on the grooved surface looked very different than that on the flat surface, as can be seen from Figure 3(d). The parallel channel like frost structure can be seen more clearly from Figure 3(e). Frost structure on the microgrooved surface at this point of time looked slightly more irregular with frost flakes growing in all directions in a random manner than the frost structure on the flat surface.

As the frost deposition is continued, the difference in the frost pattern and structure on the grooved and plain surface became slightly less distinguishable as can be seen from Figures 3(f) - (h). Figure 3(g), taken at 100 min of frost formation by a Nikkor lens instead of the microscopic lens, gives the long shot view of the frost structure on both kinds of surfaces. The left half of the surface looks irregular and less dense even from this view and difference in the frost pattern could still be identified. Shape and distribution of the frost crystals on the grooved surface after a frosting period of 160 minutes is shown in figure 3(h).

Comparison of Condensate Retention characteristics

After growing frost for 3 hours, defrosting process was carried out by self-defrost and electric heating methods and defrosting was terminated when the plate temperature reached

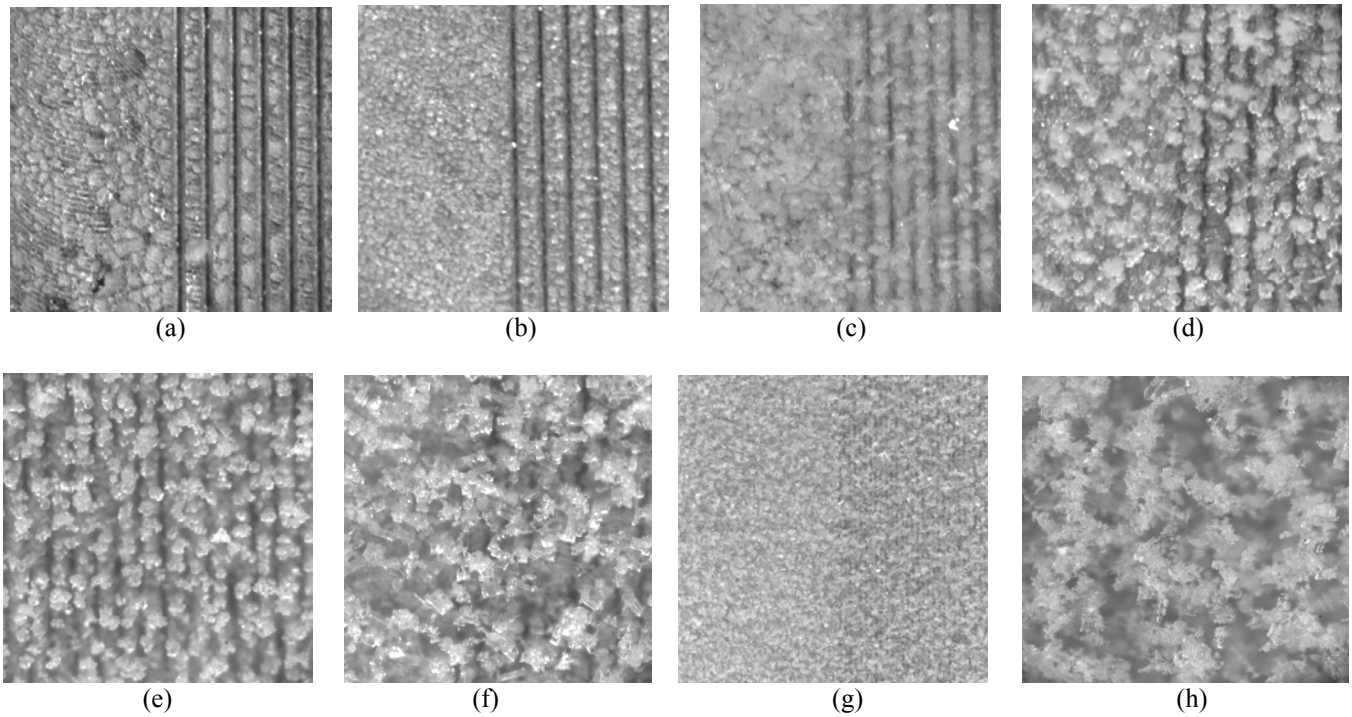

Figure 3 Images comparing the difference in frost structure on microgrooved (right half) and plain brass surfaces (left half) at a relative humidity of 80% and plate temperature of -25^{0}C under forced convection condition. The images are taken at different time intervals of a) 23 min b) 35 min c) 45 min d) 60 min, e) 60 min (frost on the microgrooved portion only) f) 90 min g) 100 min (long shot) h) 160 min (microgrooved surface only). Frost structure after a longer period of frosting shows slightly less distinguishable features between plain and microgrooved brass surfaces, as can be seen from the images 3(f) - (h).

a value of ≈ 5^{0}C. Total amount of frost accumulated on the sample at the end of frosting period and the amount of condensate drained from the surface during defrosting was measured by a direct mass measurement system, and these measurements were also verified by collecting the retained water and weighing on another high precision balance.

Drainage of the frost melt water from the surface of 7 microgrooved and 1 flat brass samples were examined and the result are shown in Table 2. The results are expressed in terms of the condensate retention ratio which is the ratio of the mass of condensate retained on the sample after defrosting (M_R) to the total mass of frost that was accumulated at the end of frosting period (M_T). The amount of condensate retained on the microgrooved surfaces was significantly lower than the plain brass surface under the same test condition, as can be seen from the results in table 2. Reduction in the amount of condensate retained on the microgrooved surface was in the range of 5.6% to as high as 71% than the plain surface. In our tests, higher reduction in the condensate retention was seen for the defrost cases when the defrosting was carried out by electrically heating the substrate. Under all the conditions, microgroove sample BR-7 (with a groove depth of ≈ 60 μm, groove width of 127 μm and pillar width of 190 μm) exhibited better water drainage among all the microgrooved samples.

There are few possible candidates for this considerable improvement in the condensate retention characteristics of the surfaces with parallel microgrooves. The difference in the frost structure and frost formation pattern as well as the different nature and characteristics of condensate drainage

Table 2 Condensate retention data for 2 defrosting methods

Sample	Reduction in condensate retention over baseline (%)	
	Self Defrost	Electric defrost
BR-1	11.3	41.3
BR-2	34.1	42
BR-3	7.8	38.5
BR-4	5.6	37.8
BR-5	6.8	29.6
BR-6	19	31.9
BR-2	34.1	42
BR-7	56.2	70.9

pattern during defrosting between the microgrooved and plain brass surfaces possibly played very crucial role. Again, anisotropic wetting behaviour of the microgrooved samples might have also affected the condensate drainage of the frost melt. In addition to that, ice-slashing (sliding of ice-water mixture) from microgrooved surface with long chucks of ice slide down along the groove before melting was possibly also another contributing factor.

The microgrooved samples showed highly anisotropic wetting which was found to significantly affect the condensate drainage characteristics on these samples. The samples exhibiting high static contact angles in both parallel and perpendicular directions and Cassie wetting regime also

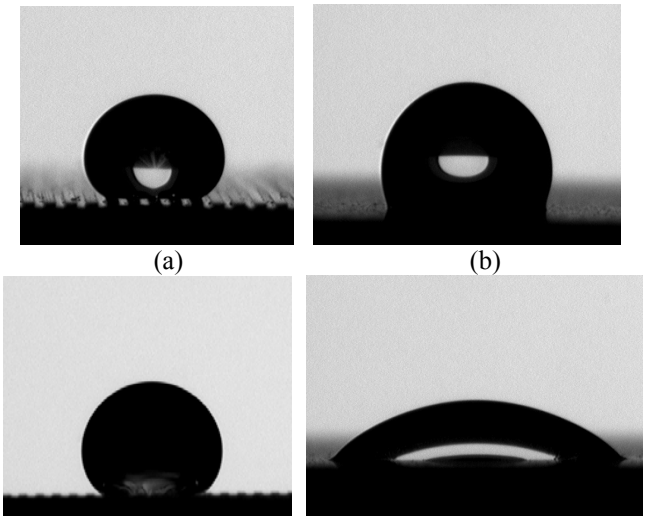

(a) (b) (c) (d)

Figure 4 Droplet in Cassie state on sample BR-7 when viewed from a) parallel and b) perpendicular direction and that in Wenzel state as viewed from c) parallel (on sample BR-1) and d) perpendicular direction of the groove (on sample BR-4).

manifested better condensate drainage.

Sample BR-7 showed the maximum condensate drainage in all cases and had high SCA of 142.94^0 and 115.51^0 in the parallel and perpendicular directions respectively. Wetting anisotropy, on the other hand, was lowest for this sample with a value of 27.43^0. Sample BR-2 performed 2nd best in terms of condensate drainage and SCA on this sample was 145.66^0 and 85.20^0 in the parallel and perpendicular directions respectively, with contact angle anisotropy of 60.46^0. These two samples also exhibited Cassie wetting regime while the other samples were found to be in Wenzel wetting mode when a droplet was gently placed on them.

Very high degree of distortion of the water droplets was found for samples exhibiting Wenzel state and the droplets assumed a flat, elongated shape when viewed from the perpendicular direction. This was due to the pinning of the three phase contact line by the groove edge and the absence of energy barrier to wetting in the parallel direction. Droplets in the Cassie state had more spherical shape and the droplet elongation was significantly lower than the droplets in Wenzel wetting regime. Figures 4(a) - 4(d) show the shape of water droplets in Cassie state on sample BR-7 and Wenzel state on sample BR-3, when viewed from parallel and perpendicular directions of the grooves. As can be seen from these images, drop on the sample BR-7 was resting on pillars only, had an air pocket under the droplets and assumed a nearly spherical shape. The droplet showing Wenzel state on sample BR-3, on the other hand, sank down the pillars and spread along the grooves to assume a much elongated shape. This anisotropic wetting and differential spreading of the liquid on different samples possibly contributed to the difference in the water retention behaviour observed among different microgrooved samples.

Variation of SCA among the microgrooved samples in the parallel direction was about 13^0 and that in the perpendicular

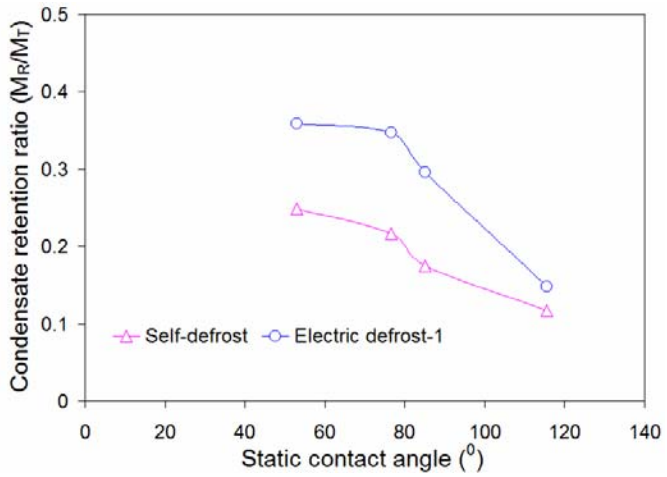

Fig. 5 Variation of condensate retention with static contact angle in perpendicular direction, for samples with fixed groove width and height

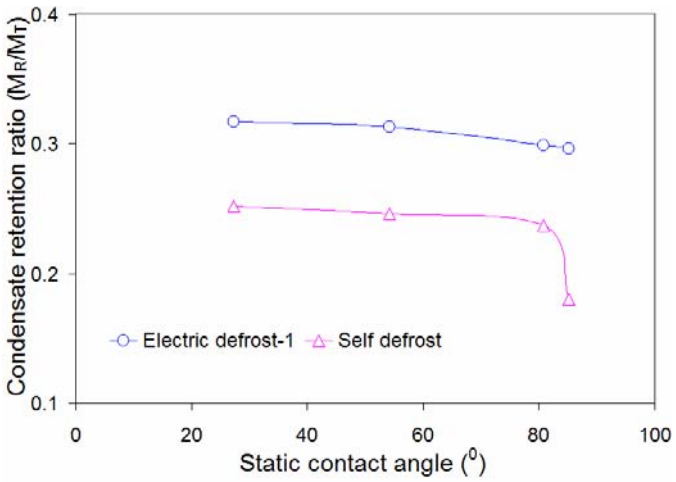

Fig. 6 Condensate retention decreases with increase in static contact angle in perpendicular direction as also seen for samples with fixed groove and pillar width.

direction (57.87^0 for samples with varying groove height and 62.46^0 for the sample with varying groove spacing). This variation in contact angle in both directions was found to significantly affect on the condensate drainage characteristics.

For samples having a fixed groove height and width, the amount of condensate retained on the sample decreased with an increase in static contact angle in the perpendicular direction. More than 50% reduction in the condensate retention was obtained as SCA increased from 53.05^0 to 115.51^0 (Figure 5). For samples with fixed groove and pillar width but varying groove height, similar improvement in condensate drainage was also found (Figure 6). Condensate retention on microgrooved samples decreased with an increase in contact angle in perpendicular direction; but the degree of variation was less than the samples with fixed groove height.

Effect of variation in SCA in parallel direction on the condensate retention characteristics of microgrooved samples

with fixed groove height and fixed groove spacing are shown in Figures 7 and 8 respectively. Water retention characteristics of the microgrooved samples were less influenced by the variation in the SCA in parallel direction. For samples with fixed groove height, water retention ratio showed a little decrease in both the defrosting methods with increase in SCA from 132^0 to 146^0. No specific trend in the water retention behaviour was observed with change in the SCA for samples having fixed groove spacing. Minimum condensate retention for both defrosting methods was obtained for the same sample (BR-7) with a SCA of $\approx 143^0$ in parallel to groove direction.

Defrosting Behaviour

Heating rate of the heat transfer surface and rate of change of frost temperature control the dynamics of frost melting and possible evaporation of the condensate. Variation in the frost surface and substrate temperature during defrosting can provide valuable information about the defrosting process and can serve as an indicator or control signal for the defrost control system [23].

Frost surface temperature was measured during the frosting and defrosting process by an infrared camera. An emissivity value of 0.9 was used for frost surface temperature measurement. These measurements were taken for various frost cycle plate temperature values and when defrosting was carried out in room temperature air. Figure 9 shows the variation of frost surface temperature with defrosting time on a microgrooved and the flat brass surface for two defrosting methods. Frost surface temperature on both kinds of surfaces had nearly equal temperatures and varied in a similar manner under the same condition.

Variation of plate and frost surface temperature of a microgrooved surface as a function of defrosting time for two defrosting methods is shown in Figure 10. Plate temperature, which was much below the frost surface temperature initially, increased at a faster rate than the frost surface temperature for both defrosting methods and they became equal near the melting point of ice.

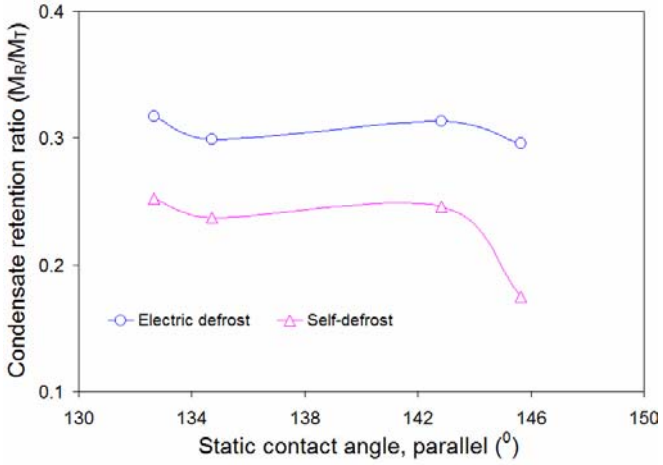

Figure 7 Amount of condensate retained on the microgrooved samples showed a slight reduction with increase in the static contact angle in the parallel direction for microgrooved surfaces with fixed groove height, but varying groove spacing

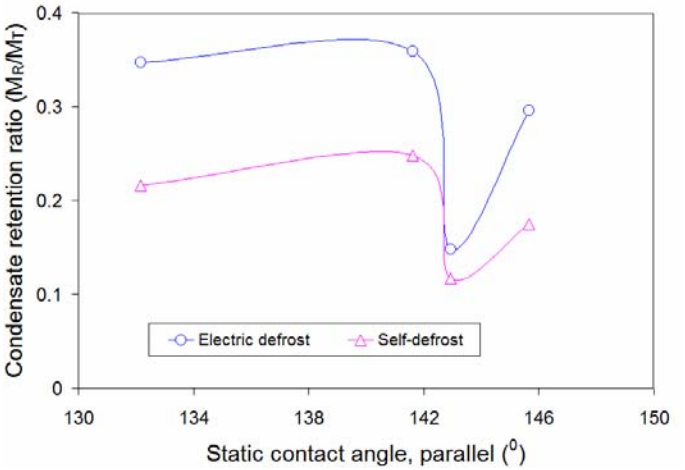

Figure 8 Variation of condensate retention ratio with static contact angle in parallel direction for microgrooved samples with fixed groove spacing, but different groove height

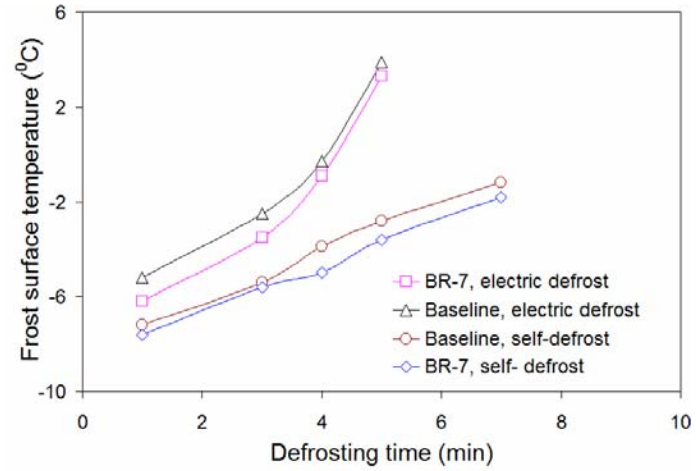

Figure 9 Variation of frost surface temperature during defrosting on a microgrooved and the flat baseline surface.

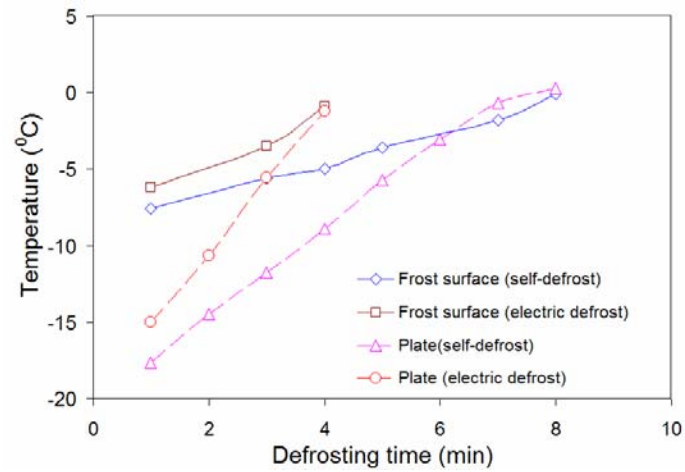

Figure 10 Frost surface and plate temperature as a function of defrosting time on a microgrooved surface for same frosting cycle plate temperature. In both defrosting methods, plate temperature during defrosting increases faster than the frost surface temperature.

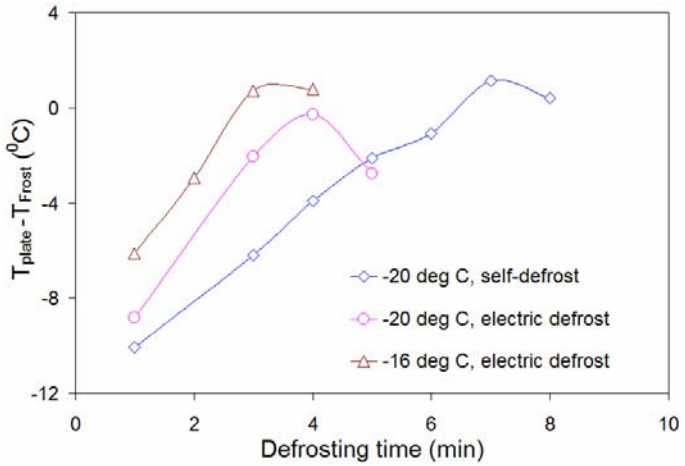

Figure 11 Difference in plate temperature and frost surface temperature decreases with defrosting time and becomes zero near the frost melting point for different frosting cycle plate temperatures and defrost methods.

Frost surface temperature measurements exhibited a sudden jump to a very high and unrealistic value when the frost surface started to melt rapidly near 0^oC. This happened as the emissivity value of 0.90 was not appropriate anymore at this stage. This sudden jump in temperature in the frost surface temperature as measured by an infrared camera could serve as a sensing input for the defrost control system.

The difference of plate and frost surface temperature as a function of time for different plate temperatures and defrosting methods is plotted in Figure 11. The difference diminished more rapidly for the electric defrost method and reached the frost surface temperature near the melting point of ice.

CONCLUSION

Condensation and frost formation pattern on vertical microgrooved and plain brass surfaces were investigated under forced convection condition in the presence of very cold air (-6^0C). Condensate retention performance of the microgrooved surfaces, fabricated by micro end-milling method, was also examined and compared with plain brass surface for two defrost methods. Frost structure on the microgrooved surface during the early stage of frost formation, with frost growing on the pillars leaving parallel empty dark lines on the grooves between them, was considerably different than those on the plain brass surface. Frost structure on the grooved surface showed more irregularity and directional crystal growth up to nearly 1.5 hrs of frost formation. For longer frosting operation, the differences in the frost structure on the grooved and plain surfaces were slightly less distinguishable. Significant improvement in condensate drainage was observed for all the microgrooved samples and up to 70% reduction in the condensate retention was achieved on these surfaces over the plain surface. Wetting behaviour of the microgrooved surface was found to have a profound impact on condensate drainage ands better drainage performance was obtained for surfaces with higher static contact angle and lower anisotropy. The variation in temperature of frost surface and brass plate during defrosting period for different defrosting method was also examined, which can serve as a potential input in defrosting control systems. Findings of this study can be very important for better management of condensate drainage from heat transfer equipments undergoing frosting/defrosting processes.

ACKNOWLEDGEMENT

We gratefully acknowledge the financial support from Air Conditioning and Refrigeration Centre (ACRC) at the University of Illinois at Urbana-Champaign.

REFERENCES

[1] Zhao B, Moore J. S, Beebe D. J., 2007 Surface –Directed Liquid Flow Inside Microchannels, *Science* 291, 1023-1026

[2] Liu L., Jacobi A. M., Chvedov D. 2009 A Surface Embossing Technique to Create Micro-grooves on an Aluminum Fin Stock for Drainage Enhancement, *J. Micromech. Microeng.* **19** (2009), pp. 35026-35034

[3] Kim J. H., Yoneya M., Yokoyama H., Tristable Nematic Liquid-Crystal Device Using Micropatterned Surface Alignment *Nature* 2002 420, 159-162

[4] Öner D., McCarthy T. J., Ultrahydrophobic Surfaces: Effects of Topography Length Scales on Wettability *Langmuir*, 2000, 16 (20), pp 7777–7782

[5] Yoshimitsu Z., Nakajima A., Watanabe T., and Hashimoto K., Effects of Surface Structure on the Hydrophobicity and Sliding Behavior of Water Droplets *Langmuir*, 2002, 18, pp. 5818-5822

[6] Morita M., Koga T, Otsuka H, Takahara A., Macroscopic-Wetting Anisotropy on the Line-Patterned Surface of Fluoroalkylsilane Monolayers, *Langmuir* 21 (2005) 911–918.

[7] Chen Y., He B., Lee J., Patankar N.A., Anisotropy in the Wetting of Rough Surfaces *J. Colloid Interface Sci.* 281 (2005) 458– 464.

[8] Sommers A. D., Jacobi A. M., Creating Micro-Scale Surface Topology to Achieve Anisotropic Wettability on an Aluminum Surface *J. Micromech. Microeng.* 2006 16 1571–1578

[9] Sommers A. D., Jacobi A. M., Wetting Phenomena on Micro-grooved Aluminum Surfaces and Modeling of the Critical Droplet Size *J. Colloid Interface Sci.* 2008 (328), 402-411

[10] Hoke, J. L., Georgiadis, J. G., and Jacobi, A. M., 2000, The Interaction between the Substrate and Frost through Condensate Distribution,' *Technical report*, University of Illinois, Urbana-Champaign

[11] Shin J., Tikhonov A. V., Kim C., Experimental Study on Frost Structure on Surfaces with Different Hydrophilicity: Density and Thermal Conductivity, *Journal of Heat Transfer* 2003, Vol. 125 (85)

[12] Lee H., Shin J., Ha S., Choi B., Lee J., Frost formation on a plate with different surface hydrophilicity, *International Journal of Heat and Mass Transfer* 47 (2004) 4881–4893

[13] Liu Z., Gou Y., Wang J., Cheng S., Frost formation on a super-hydrophobic surface under natural convection

conditions, *International Journal of Heat and Mass Transfer,* 51 (2008) 5975–5982

[14] Jhee S., Lee K. S., Kim W. S., Effect of surface treatments on the frosting/defrosting behavior of a fin-tube heat exchanger *International Journal of Refrigeration* 25 (2002) 1047–1053

[15] Narhe R. D. and Beysens D. A., Nucleation and Growth on a Superhydrophobic Grooved Surface, *Physical Review Letters*, 2004, 93, 7

[16] Narhe R. D. and Beysens D. A., Growth Dynamics of Water Drops on a Square-Pattern Rough Hydrophobic Surface, *Langmuir* 2007, *23,* 6486-6489

[17] Cassie A. B. D. and Baxter S., Wettability of porous surfaces *Trans. Faraday Soc.*, 1944, 40, 546-551

[18] Wenzel, R. Resistance of Solid Surfaces to Wetting by Water *Ind. Eng. Chem.* 1936, *28*, 988

[19] Tourkine P., Merrer M. L., and Quere D., Delayed Freezing on Water Repellent Materials *Langmuir,* 2009, 25(13), 7214–7216

[20] Super-hydrophobic film retards frost formation, He M., Wang J., Li H., Jin X., Wang J., Liu B., Song Y., *Soft Matter*, 2010, 6, 2396–2399

[21] Okoroafor E.U., Newborough M., Minimizing frost growth on cold surfaces exposed to humid air by means of cross-linked hydrophilic polymeric coatings, , *Applied Thermal Engineering* 20 (2000) 737-758

[22] Wu X. M. and R.L Webb, Investigation of possible frost release from a cold surface, *Experimental Thermal and Fluid Science*, 2001 (24), 161-156

[23] Iragorry J. and Tao Y. X., Frost Temperature Relations for Defrosting Sensing System, J of heat Transfer, 2005, 127, pp. 344-351